Angewandte
GDCh
Chemie
Eine Zeitschrift der Gesellschaft Deutscher Chemiker
www.angewandte.de

Akzeptierter Artikel

Titel: Red- and Far-Red-Emitting Zinc Probes with Minimal Phototoxicity for Multiplexed Recording of Orchestrated Insulin Secretion

Autoren: Junwei Zhang, Xiaohong Peng, Yunxiang Wu, Huixia Ren, Jingfu Sun, Shiyan Tong, Tianyan Liu, Yiwen Zhao, Shusen Wang, Chao Tang, Liangyi Chen, and Zhixing Chen

Zitierweise: *Angew. Chem. Int. Ed.* 10.1002/anie.202109510

Link zur VoR: https://doi.org/10.1002/anie.202109510

WILEY-VCH

10.1002/ange.202109510

WILEY-VCH

RESEARCH ARTICLE

Red- and Far-Red-Emitting Zinc Probes with Minimal Phototoxicity for Multiplexed Recording of Orchestrated Insulin Secretion

Junwei Zhang[+], Xiaohong Peng[+], Yunxiang Wu[+], Huixia Ren[+], Jingfu Sun, Shiyan Tong, Tianyan Liu, Yiwen Zhao, Shusen Wang, Chao Tang, Liangyi Chen and Zhixing Chen*

[*] J. Zhang[+], X. Peng[+], Y. Wu[+], Y. Zhao, L. Chen, Z. Chen*
College of Future Technology, Institute of Molecular Medicine, National Biomedical Imaging Center, Beijing Key Laboratory of Cardiometabolic Molecular Medicine, Peking University, Beijing 100871 (China)
E-mail: zhixingchen@pku.edu.cn
H. Ren[+], T. Liu, C. Tang, Z. Chen
Peking-Tsinghua Center for Life Science, Peking University, Beijing 100871(China)
X. Peng[+], L. Chen
State Key Laboratory of Membrane Biology, Peking University, Beijing 100871 (China)
H. Ren[+], C. Tang
Center for Quantitative Biology, Peking University, Beijing 100871 (China)
J. Sun, Z. Chen
PKU-Nanjing Institute of Translational Medicine, Nanjing 211800 (China)
S. Tong
School of Life Science, Peking University, Beijing 100871 (China)
S. Wang
Organ Transplant Center, Tianjin First Central Hospital, Nankai University, Tianjin 300192 (China)
[+] These authors contributed equally to this work.
Supporting information for this article is given via a link at the end of the document.

Abstract: Zinc biology, featuring intertwining signaling networks and critical importance to human health, witnesses exciting opportunities in the big data era of physiology. Here, we report a class of red- and far-red-emitting Zn^{2+} probes with K_d values ranging from 190 nM to 74 μM, which are particularly suitable for real-time monitoring the high concentration of Zn^{2+} co-released with insulin during vesicular secretory events. Compared to the prototypical rhodamine-based Zn^{2+} probes, the new class exploits morpholino auxochromes which eliminates phototoxicity during long-term live recording of isolated islets. A Si-rhodamine-based Zn^{2+} probe with high turn-on ratio (> 100), whose synthesis was enabled by a new route featuring late-stage N-alkylation, allowed simultaneous recording of Ca^{2+} influx, mitochondrial signal, and insulin secretion in isolated mouse islets. The time-lapse multicolor fluorescence movies and their analysis, enabled by red-shifted Zn^{2+} and other orthogonal physiological probes, highlight the potential impact of biocompatible fluorophores on the fields of islet endocrinology and system biology.

Introduction

Zinc (Zn^{2+}) plays a critical role in both physiological and pathological processes such as signal transduction[1], apoptosis[2], and gene transcription and expression[3]. Most of Zn^{2+} in cells is tightly bound to proteins to serve as structural components or catalytic centers of enzymes, while another fraction is free or weakly chelated with small molecules for signaling purposes in multiple organs[4]. Zn^{2+} is heterogeneous in space, yet its dynamics can be fast or even transient, as in neurophysiological[5], reproductive[6], and pancreatic secretory processes[7]. Investigators of Zn^{2+} physiology are therefore challenged to develop bioanalytical methods to fully unveil the map of dynamic Zn^{2+} homeostasis. Since the 2000s, fluorescence imaging has emerged as an indispensable tool to study Zn^{2+} biology, thanks to the coevolution of microscopy and indicators. To date, a series of fluorescent probes, including small-molecule probes, genetically encoded indicators and hybrid probes[8], with different affinities and emission wavelengths have been developed to detect Zn^{2+} in living system, extending the cutting-edge in Zn^{2+} biology[9] (Figure 1a). The ever-developing toolbox of Zn^{2+} probes, however, can be further upgraded in three ways: (1) In contrast to numerous bis(pyridylmethyl)amine (DPA) -derived Zn^{2+} probes with nM affinity, probes for the μM to mM range are relatively rare. Zn^{2+} concentrations span around 8 orders of magnitude, down to 10^{-10} M in cytoplasm[10] and up to 10^{-2} M in some vesicles[11]. Unusually high Zn^{2+} in insulin secretory granules[12] (~ 20 mM) and synaptic vesicles[5] (~ 10 - 30 μM) suggests its importance in physiology of excitable cells. (2) The existing toolbox of red- and far-red-emitting Zn^{2+} probes[9d, 9f, 9g, 13] need to be further expanded to be used in combination with the plentiful indicators in green and red channels (e.g., GCaMP and RCaMP for calcium (Ca^{2+}) signaling) for studying complex signaling networks. (3). Long-term, high spatial/temporal resolution fluorescence imaging probes, bearing superior photostability and minimal phototoxicity, are not yet readily available but vitally important. The core optical motif of the Zn^{2+} probes often exploit the classical chromophores for confocal-imaging, but the chromophores are more phototoxic or less biocompatible[14]. These classic probes cannot meet the challenge of "4D physiology" in the big data era, where long stretches of high-resolution video in multiple channels are recorded to generate the full picture of a molecular signaling network.

10.1002/ange.202109510

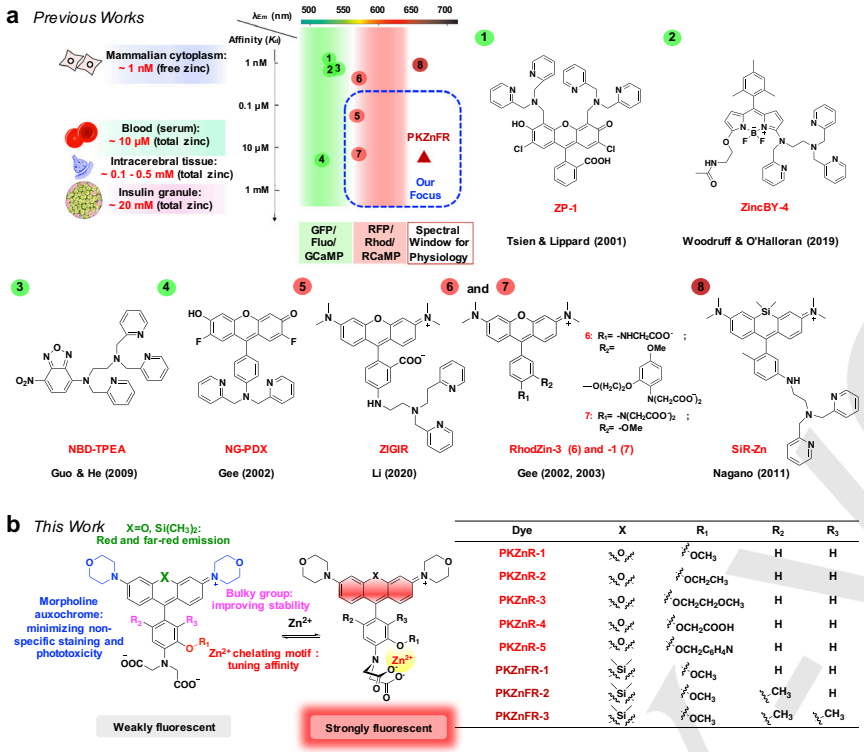

Figure 1. The history of Zn^{2+} fluorescent probes and the design of the PK Zinc Family. (a). A map summarizing the state-of-the-art Zn^{2+} probes with different emission wavelengths and binding affinities for physiological studies in various tissues. (b) Design strategy and chemical structures of the **PK Zinc Family**, featuring red-shifted emission and enhanced biocompatibility for studying dynamic Zn^{2+} in the μM range.

β-cell endocrinology is a field that would particularly benefit from a new generation of Zn^{2+} probes. In the vesicles of β-cells, Zn^{2+} co-crystalizes with insulin in the form of 6-insulin-2-Zn-hexameric complexes, giving rise to a distinctively high concentration of Zn^{2+} (~20 mM) in secretory granules[12]. After glucose stimulation, Zn^{2+}/insulin complex is released from vesicles in a rapid and heterogeneous manner[15]. The malfunction of such process will lead to insulopathic disease[12]. Thanks to modern microscopy that offers high spatial/temporal resolutions, insulin secretion has been routinely imaged in cell clusters or intact islets using Zn^{2+} probes. Prior efforts on probe development include cell-permeable Zn^{2+} probes (DA-ZP1[16], ZIGIR[9e]) for total granules, plasma membrane-inserted probes (ZIMIR[17]) for secreting cells, and membrane-impermeable extracellular probes (FluoZin-3[18] and RhodZin-3[9f, 15]) that highlight opening vesicles as fluorescent puncta which precisely correlates to individual fusion events of insulin granules (Figure 2b). The cutting edge of islet biology has moved from the cell to the tissue level, in order to fully understand the regulation of β-cell secretion in the context of a whole islet. However, the general challenges for probes remain: (1) In the complex environment of the islet, probes must have high turn-on ratios to increase sensitivity and appropriate K_d values to ensure the accuracy of analysis. (2) Red- and far-red Zn^{2+} probes are ideal, as Ca^{2+} signals in islets, commonly monitored by genetically-encodable GCaMP, must be recorded simultaneously for studying signal networks. (3) Insulin release is an elaborately regulated tri-phasic process which lasts for more than an hour. While modern microscopes (i.e., spinning disk confocal) are well equipped for time-lapse imaging, the recording of such a long process is eventually limited by the photo-biocompatibility of the probes. In our opinion, these challenges represent general concerns in the ion probe field. Bridging these technological gaps could provide a holistic view of orchestrated signaling in the islet, and at the same time shed light on a broad community of bioinorganic chemistry.

Herein we present a class of red- and far-red-emitting rhodamine-based Zn^{2+} probes with K_d values spanning the μM range. The new class, named **PK Zinc Red** and **Far Red (PKZnR and PKZnFR)**, is particularly suitable for imaging the high concentrations of Zn^{2+} released during vesicular secretory events in real-time (Figure 1b). Compared to the prototypical rhodamine-based Zn^{2+} probes, this new class exploits hydrophilic morpholino auxochromes, thus eliminating phototoxicity during live recording from isolated islets. The library of red-emitting Zn^{2+} probes with different chelating motifs has different binding affinities (K_d values from 190 nM to 74 μM), thus enabling the recording of Zn^{2+}/insulin co-release in both cell clusters and intact islets. Furthermore, we developed far-red-emitting Zn^{2+} probes with a novel synthetic strategy involving a transient protective group. We demonstrate four-color simultaneous recording of Ca^{2+}, mitochondrial, nuclear, and Zn^{2+}/insulin secretion signals in isolated islets. These **PK Zinc** probes revealed the orchestrated and heterogeneous regulation of secretion, underscoring the growing importance of photo-biocompatibility, signal multiplexing, and molecular tunability in the big data era of 4D physiology at the tissue level.

Results and Discussion

Morpholino auxochromes on a rhodamine scaffold minimize non-specific staining and phototoxicity during the recording of Zn^{2+}/insulin co-release in isolated islets.

To develop ideal probes meeting the new criteria, we first evaluated a classic red probe for imaging a whole isolated islet. **RhodZin-1**, a prototypical red Zn^{2+} probe with a binding affinity of 23 μM, is considered suitable for *ex vivo* recording of fusion events[9d]. **RhodZin-1** belongs to the impermeable class of probes, therefore is expected to induce minimal phototoxicity compared to its cellular-localized counterparts (DA-ZP1[16] and ZIGIR[9e]). We timed our video recordings from the addition of 18.2 mM glucose and expected to record Zn^{2+}/insulin co-release spanning long-term imaging. However, during a half-hour of *ex vivo* recording, we still observed a gradual accumulation of **RhodZin-1** into the cells (Figure 2e and Movie 1), giving rise to non-specific staining in cellular compartments (Figure 2g and 2k). Consequently, the phototoxicity of **RhodZin-1** predominated and triggered apoptotic

10.1002/ange.202109510
WILEY-VCH

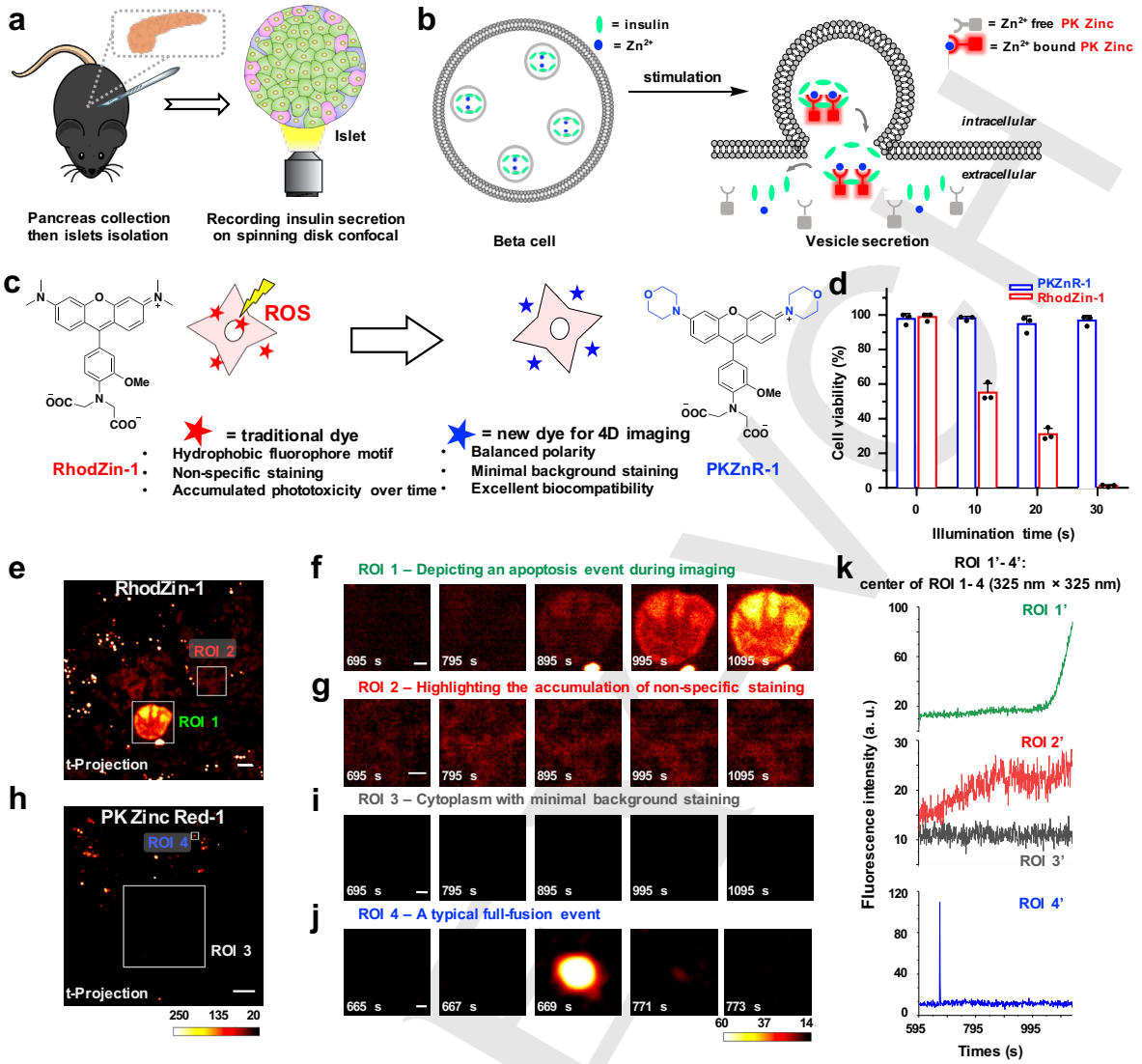

Figure 2. Morpholino auxochromes on a rhodamine scaffold minimize non-specific staining and phototoxicity during the *ex vivo* recording of Zn^{2+}/insulin co-release in mouse islet. (a). Protocol to visualize Zn^{2+}/insulin co-release in intact islets. (b). Mode of action of **PK Zinc** for reporting local Zn^{2+} elevation in the extracellular space during exocytotic insulin granule fusion. (c). Chemical structures of **RhodZin-1** and **PKZnR-1**, schematic diagram of their interaction with cells. (d). Phototoxicity of **RhodZin-1** and **PKZnR-1** (10 μM) on HeLa cells, measured by cell viability after green light illumination (568 nm, 4.1 W/cm^2). (e). The maximum-intensity t-projection (540 s) of an islet stained with **RhodZin-1** (10 μM). (f). Time-dependent images of ROI 1 depicting an apoptosis event. (g). Time-dependent images of ROI 2 highlighting the accumulation of non-specific staining. (h). The maximum-intensity t-projection (540 s) of an islet stained with **PKZnR-1** (10 μM). (i). Time-dependent images of ROI 3 showing clean cytoplasm with minimal background staining. (j). Time-dependent images of ROI 4 showing a typical full-fusion event. For (e) and (h), scale bar = 5 μm; for (f), (g) and (i), scale bar = 2 μm; for (j), scale bar = 0.2 μm. Imaging conditions for (e) to (j): 561 nm laser illumination, 0.3 W/cm^2, exposure time 100 ms. (k). Time courses of fluorescence of ROI-1' through ROI-4' (325 nm × 325 nm).

staining patterns in the nucleus as time-lapse imaging continued (Figure 2f and 2k). The background staining and apoptotic event were routinely observed in several independent repeated experiments (Figure S11). We speculated that this appearance was due to the considerable liposolubility of **RhodZin-1**. The hydrophobic upper half of **RhodZin-1** and the ionic chelator rendered the molecule a detergent-like behavior to interact with membranes. Inspired by a classical strategy in medicinal chemistry, we proposed to tune the polarity balance of the rhodamine probe with morpholino groups (Figure 2c). Compared to the other reported strategies which increase the hydrophilicity of probes by sulfonation[19], morpholino auxochromes neither change the net charge nor increase the synthetic difficulty. Therefore, we synthesized the morpholino auxochrome-based rhodamine probe, **PKZnR-1**. The molecule exhibited increased hydrophilicity (confirmed by the retention time on C18 column of liquid chromatography, Figure S10) which reduced its interaction with the cell membrane (Figure 2c). Firstly, we evaluated the phototoxicity of two probes on HeLa cells. **RhodZin-1** caused significant phototoxicity after 30 s of continuous green light illumination (568 nm, 4.1 W/cm^2) while most **PKZnR-1** treated cells were still alive (Figure 2d). We further applied **PKZnR-1** to islet imaging. Non-specific staining in cells was eliminated when using **PKZnR-1** for islet imaging (Figure 2h and Movie 1). The background fluorescence intensity in the cytoplasm did not increase during long-term imaging (Figure 2i and 2k), nor did we find photo-induced apoptosis. The minimized non-specific

10.1002/ange.202109510

staining and phototoxicity ensured the recording of physiologically relevant fusion events (exemplified in Figure 2j and 2k). Furthermore, we incubated the two probes with islets for 1000 s in the dark. Only non-specific staining signal, but not apoptotic signal, was observed in islets treated with **RhodZin-1.** After laser illumination, apoptotic signal was constantly observed (Figure S12). Moreover, there was no significant difference in dark toxicity between the two probes on HeLa cells (Figure S13). Those evidence further pinpointed the main difference between the two probes to cell permeability-rendered phototoxicity, not dark toxicity. Overall, we established the use of a morpholino auxochrome as a successful strategy for minimizing the phototoxicity of a Zn^{2+} probe.

Modular rhodamine chemistry enables the installation of diverse chelating groups for tunable Zn^{2+} affinity.

The biological pool of Zn^{2+} features a high heterogeneity in space, with concentrations spanning the nM to mM ranges. We sought to elaborate morpholino probes for various applications by systematically tuning their affinity to Zn^{2+}. **RhodZin-1**, featuring a 2-methoxyaniline-N, N-diacetate chelating group, was selected as a prototype for further engineering. Our design retained the main chelating groups (N, N-diacetic acid) while changing the structure of the side-chain, so as to tune the affinity on the premise of maintaining the selectivity of Zn^{2+}. **PKZnR-1** was the lead structure of this morpholino class, with methoxy as the side chain. In **PKZnR-2**, we substituted the methoxy group with the more sterically hindered ethoxy group to reduce affinity. We increased the chelating sites at the side-chain to devise methoxyethoxy-substituted **PKZnR-3** and o-aminophenol-N, N, O-triacetic acid (APTRA)[20]-based **PKZnR-4**. In **PKZnR-5**, a 2-pyridylmethyl group was installed at the side-chain, as this pyridine-containing chelator has been reported to be sufficiently selective and have a high affinity[21]. All these molecules were synthesized via a modular condensation-oxidation reaction to assemble the rhodamine core, followed by deprotection to liberate the chelator motif (Scheme S1). The straightforward chemistry enabled the facile preparation of **PKZnR** probes for characterization.

The photophysical properties of these probes was tested *in vitro*, by measuring Zn^{2+} -dependent change in fluorescence (Figure 3a), absorption (Figure 3a (inset)), titration (Figure 3b), the effect of pH (Figure 3c) and selectivity against other divalent cations and selected peptides (Figure 3d). The **PKZnR** family generally exhibited excellent Zn^{2+} selectivity over other biologically relevant divalent ions or selected peptides, while offering diverse affinity to Zn^{2+} spanning 190 nM to 74 μM (Figure 3e, detail in Figure S1-S5, fitting equation in Supporting Information). It is worth noting that **PKZnR-3** presented a lower affinity than **PKZnR-1**, suggesting that the steric hindrance effect of this side-chain was greater than that of the additional methyl ether. The probes in this family demonstrated a 1:1 metal-to-ligand complex ratio, which was confirmed by Job's plots (Figure S1-5e). Because the chelating group is directly coupled to the fluorophore, the effective Photoinduced electron Transfer (PeT) quenching gave considerable "turn-on" responses of the probes to Zn^{2+} (from 21 to 96, except **PKZnR-4**). When the pH value changes in the range of 5.0 to 8.0, the fluorescence of **PKZnR** probes in the Zn^{2+} free and the Zn^{2+} bound form does not change significantly. These impressive properties encouraged us to explore their applications in Zn^{2+} biology.

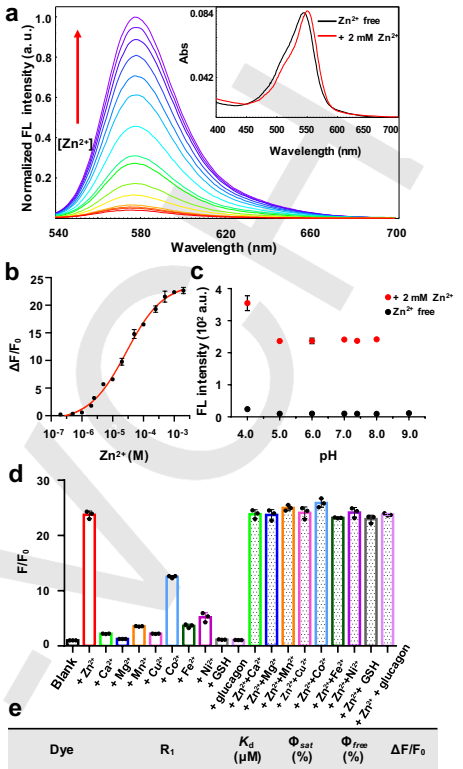

Dye	R_1	K_d (μM)	Φ_{sat} (%)	Φ_{free} (%)	$\Delta F/F_0$
PKZnR-1	-OMe	28	6.2	0.24	23
PKZnR-2	-OEt	33	5.9	0.24	21
PKZnR-3	$-O(CH_2)_2OCH_3$	74	4.4	0.17	28
PKZnR-4	$-OCH_2COOH$	0.66	9.8	2.4	3.6
PKZnR-5		0.19	9.0	0.11	96

Figure 3. Characterizations of PKZnR 1-5 *in vitro*. (a). Emission spectra of **PKZnR-1** (1 μM) in the presence of various concentrations of free Zn^{2+} (0 to 2 mM). (Inset) Absorption spectra of **PKZnR-1** (1 μM) in the presence of 0 and 2 mM free Zn^{2+}. (b). Zn^{2+} titration of **PKZnR-1** (1 μM) as measured from its emission at 580 nm. (c). pH dependence of fluorescence for **PKZnR-1** in 0 and 2 mM free Zn^{2+}. Formation of a white precipitate was observed after Zn^{2+} addition at pH 9.0, fluorescence intensity values under these conditions were therefore not measured. (d). Selectivity of **PKZnR-1** for Zn^{2+} compared to other divalent cations and peptides. Zn^{2+}, Ca^{2+}, Mg^{2+}, Mn^{2+}, Cu^{2+}, Co^{2+}, Fe^{2+}, Ni^{2+}, GSH (1 mM) and glucagon (10 μM) were added to 1 μM **PKZnR-1**. (e). Photophysical properties of **PKZnR 1-5**. All measurements were performed in buffers containing 100 mM HEPES (pH 7.4, I ($NaNO_3$) = 0.1) and 0.1% DMSO as a cosolvent at 25 °C. At free Zn^{2+} concentrations of < 0.1 μM, 10 mM nitrilotriacetic acid (NTA) was added to chelate the high concentration of total Zn^{2+}. Zero Zn^{2+} measurements were made in the presence of 10 μM TPEN. The excitation wavelength was 520 nm. Error bars denote SD; n=3.

PKZnR family covers the detection of Zn^{2+}/insulin co-release from β-cell clusters to intact mouse and human islets.

We first screened the **PKZnR** family to detect insulin granule exocytosis on pancreatic β-cell clusters. Such cellular-level imaging differs from islet imaging, as isolated cells lose their environmental niche and communicational signals, and secreted contents are extensively diluted into the medium. Out of the five probes prepared, only **PKZnR-5**, the strongest binder with a pyridyl group, efficiently highlighted insulin granule exocytosis in mouse β-cell clusters (Figure 4a and S14). The results showed that the concentration of Zn^{2+} in the extracellular space of cell clusters was much lower than that of intact islets. After glucose stimulation, additional fluorescent puncta appeared, which represented fused insulin granules. Sequential addition of N, N, N', N'-tetrakis(2-pyridinylmethyl)-1,2-ethanediamine (TPEN, 50

10.1002/ange.202109510

μM) quenched the fluorescence of these puncta (Figure 4a ,4b and Movie 2), suggesting the specific and reversible binding of **PKZnR-5** to Zn^{2+}. A similar pattern of insulin granule exocytosis was recorded in human cell clusters (Figure S15 and Movie 2). Moreover, **PKZnR-5** distinguished different types of fusion events including full, short-lived and long-lived fusion in mouse β-cell clusters (Figure S16). Such intricate behaviors, while consistent with the previous report acquired using **RhodZin-3**[15], can now be monitored over a prolonged window without severe phototoxicity (Figure S17e). Thus, **PKZnR-5** offers a less photo-damaging solution for cellular studies of insulin secretion.

We next systematically tested the **PKZnR** family in *ex vivo* recordings of Zn^{2+}/insulin co-release in intact islets (Figure S17). **PKZnR-2** accumulated in cytoplasmic organelles (Figure S17c), while the other four probes gave characteristic punctate patterns. We recommend **PKZnR-1** as the ideal reagent in this application, because its K_d value matched with the concentration of Zn^{2+} in the surrounding environment of islets after stimulation by glucose, therefore ensuring the accuracy of detection.

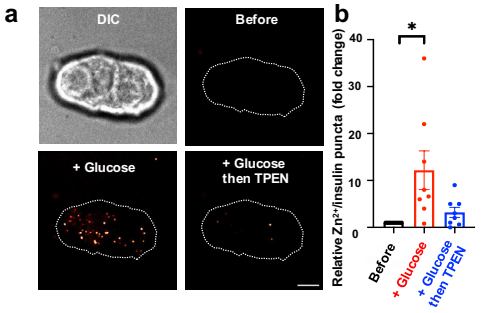

Figure 4. PKZnR-5 highlights Zn^{2+}/insulin co-release in mouse β-cell clusters. (a). Representative confocal images of **PKZnR-5** (10 μM) highlighted Zn^{2+}/insulin co-release before (left upper for bright-field image and right upper for fluorescence image) and after (left lower) glucose (18.2 mM) stimulation for 10 min, and then chelated by TPEN (50 μM, right lower) for another 10 min. Scale bar = 10 μm. (b). The fold change of numbers of fusion events under glucose stimulation in different cell clusters. Error bars denote SEM, n=8 cell clusters. ($p^* < 0.05$, t-test).

It is commonly accepted that insulin secretion is defective in patients with type 2 diabetes[22]. Given that **PKZnR-1** highlighted insulin granules within islets, we tested the potential of this experiment as an assay for screening drugs. When stimulated by 11 mM glucose, 326 ± 171 fusion events were identified within intact mouse islets (Figure 5a, b and e). The addition of forskolin, an insulin secretagogue that elevates the cytosolic cAMP concentration[23], induced 972 ± 325 fusion events (Figure 5c and e). Treatment with diazoxide, an ATP-sensitive potassium channels activator[24] to abolish glucose-stimulated insulin secretion, reduced the number of fusion events to 3 ± 1 (Figure 5d and e). These results suggest that the whole islet imaging assay using **PKZnR-1** is sensitive enough to report the dynamic changes of insulin secretion, promising a high-throughput method of screening molecules for treating insulopathic diseases, such as type 2 diabetes and hyperinsulinemia.

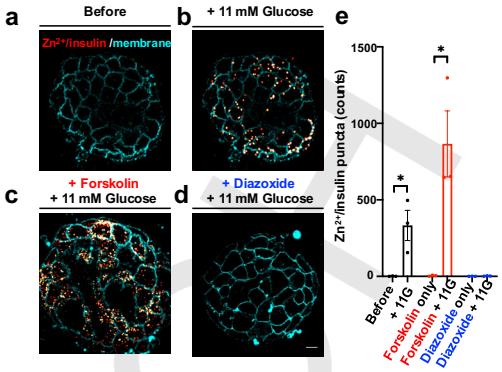

Figure 5. PKZnR-1 is capable of *ex vivo* recording of Zn^{2+}/insulin co-release in intact mouse islets under chemical stimulations. Representative examples of islet secretion before stimulation (a, 400 s) or evoked by 11 mM glucose (b,1000 s), 11 mM glucose in the presence of 1 μM forskolin (c, 1000 s), and 11 mM glucose in the presence of 250 μM diazoxide (d, 1000 s). Hot-red puncta represent fusion events during the recording time. The plasma membrane of individual cells is highlighted with **FM 4-64** dye (10 μM, cyan). Scale bar = 10 μm. (e). Numbers of fusion-event under different chemical stimulations. Error bars denote SEM, n=3 islets. ($p^* < 0.05$, t-test).

Given that **PKZnR-1** is good for detecting the exocytosis of mouse insulin granules, we also used it to detect the native insulin granules of human islets, in which genetic manipulation is not practical. Similar to mouse islets, after high glucose stimulation for ~4 min, fluorescent puncta emerged in a portion of cells (Figure 6a and Movie 3), demonstrating the native insulin secretion. Moreover, fusion events in human islets also exhibited all three types of fusion mode (Figure 6b), which indicates the conservation of insulin release regulation from mouse to human[15]. Taken together, these results show that low affinity, biocompatible **PKZnR** dyes are suitable for monitoring insulin release within intact mouse and human islets.

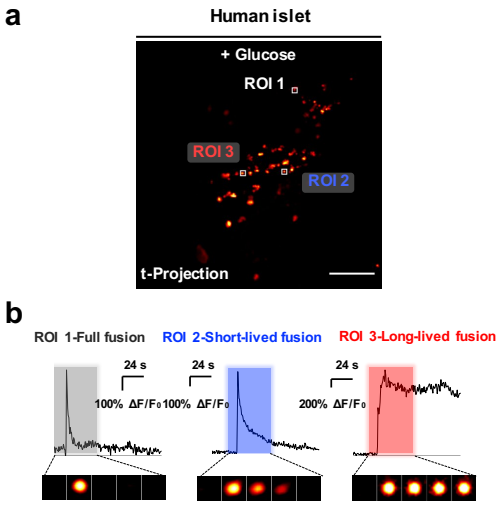

Figure 6. PKZnR-1 reveals three types of Zn^{2+}/insulin fusion mode in a human intact islet. (a). The maximum-intensity t-projection (500 s) of **PKZnR-1** (10 μM)- treated islet stimulated with 18.2 mM glucose. Scale bar = 10 μm (b). The time course of **PKZnR-1** fluorescence at the center of ROI-1 through ROI-3 (540 nm × 540 nm) shows the three fusion modes. Montages show each consecutive image series at 16 s/frame.

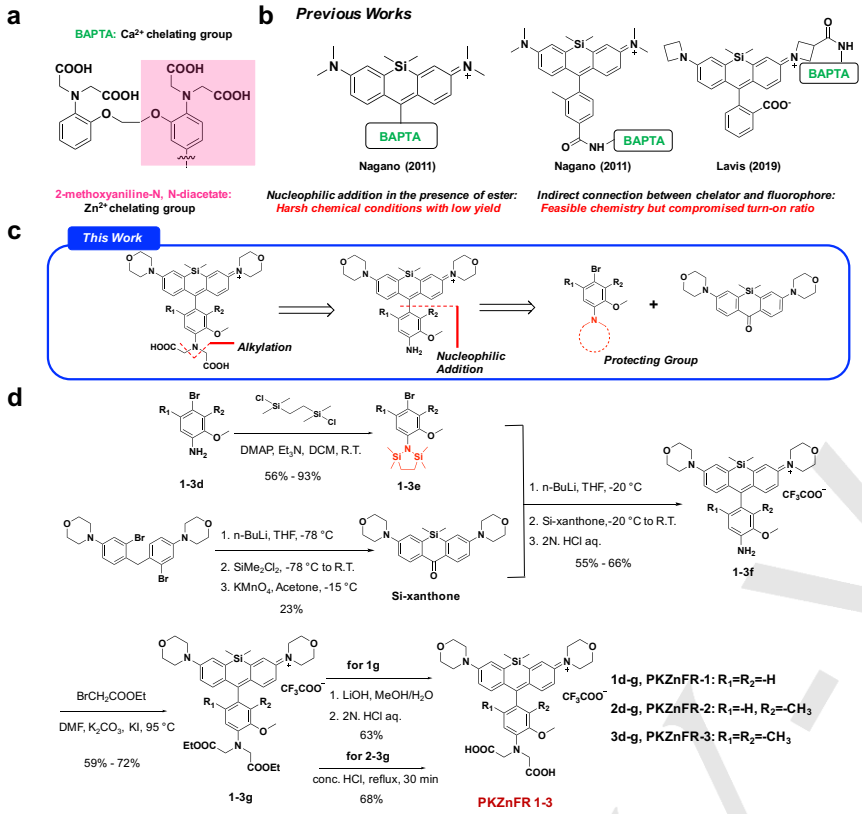

Scheme 1. Synthesis of PKZnFR 1-3. (a). Chemical structure of BAPTA, a Ca^{2+} chelator which inspired the Zn^{2+} chelator, 2-methoxyaniline-N, N-diacetate. (b). Structures of BAPTA-based Ca^{2+} indicators on a Si-rhodamine scaffold. (c). Retrosynthetic analyses of **PKZnFR 1-3**, highlighting a strategic application of late-stage N-alkylation. (d). Synthetic route of **PKZnFR 1-3**.

A Strategic late-stage N-alkylation enables practical synthesis of Si-rhodamine-based Zn^{2+} probes.

We next endeavored to expand the morpholino rhodamine family to far-red-emitting Zn^{2+} probes. Far-red channel is useful as a complementary channel to green and red for multicolor imaging, especially in physiological studies. While genetically-encoded fluorescent indicators have prevailed over the green and red channels, the far-red window is dominated by synthetic probes that have advantages in brightness and flexibility. Consequently, metal probes based on Si-rhodamine are rapidly emerging in spite of the challenges posed by their synthesis[9g, 25].

The first-generation Si-rhodamine-based cation probes featured a direct connection between the chelator and the rhodamine core (Scheme 1a and 1b). However, the inevitable strongly-reactive organolithium species were barely compatible with carbonyl chelators, giving rise to harsh reaction conditions with poor yields[25a]. A recent variation on Si-rhodamine-based Ca^{2+} probes exploited an indirect linking strategy that connected the chelator to the fluorophore through an amide bond (Scheme 1b), making the synthesis less cumbersome[25b]. However, the lone electron pair on the nitrogen atom of the chelator could no longer fully quench the fluorophore through the PeT mechanism, leading to compromised turn-on ratios.

In order to solve these problems, we designed a new synthetic route to create the **PKZnFR** family (Scheme 1c), featuring a late-stage N-alkylation to avoid nucleophilic addition in the presence of ester. A transient protecting group: 1,2-bis(chlorodimethylsilyl)ethane was used to protect aniline during the Li-Br exchange reactions[26]. The previously developed bulky-protection was inherited to block nucleophilic attack on the 9 position, ensuring chemical stability of the products[27]. Practically, compounds **1-3e**, bearing transiently protected aniline, were subjected to Li-Br exchange, followed by nucleophilic addition to the morpholino Si-xanthone. The reactions were quenched by dilute hydrochloric acid solution, in which the protecting group was removed in one-pot. Then the N-alkylation with ethyl bromoacetate was carried out. Final deprotection of esters gave **PKZnFR 1-3** (Scheme 1d). The new strategy greatly improved the overall yield, enabling the preparation of final products at the scale of tens of milligrams, making ^{13}C NMR characterization possible.

The **PKZnFR** family had absorption and emission maxima at 654 and 676 nm, fitting perfectly with the far-red (Cy5) channel on fluorescence microscopes (Figure 7a). Notably, while their affinities for Zn^{2+} were similar to **PKZnR-1** (~ 30 μM) (Figure 7b), their fluorescence turn-on ratios were > 100 (Figure 7d, detail in Figure S6 - S8). Bulky groups successfully enhanced the stability of Si-rhodamine probes in pH 7.4 HEPES buffer, suppressing their based-induced degradation (Figure 7c and S9). Both **PK ZnFR-2** and **3** exhibited minimal background staining in islet *ex vivo* imaging assays (Figure S18). Overall, we recommend **PK ZnFR-3** as the best choice of this family, featuring high serum stability, minimal non-specific background, and superior fluorescence turn-on signal.

Far-Red PK Zinc probe enables 4D imaging of the signaling networks that regulate insulin secretion in mouse islets.

Insulin secretion is a highly dynamic and multi-tiered process regulated by complex mechanisms. Briefly, glucose transported into β-cells is metabolized in mitochondria to generate ATP. The increased ATP/ADP ratio in cytosol closes ATP-sensitive potassium channels, which leads to depolarization of the cell membrane and opening of voltage-gated calcium channels, thereby allowing the flow of calcium into the cell. Finally, the rise of cytosolic Ca^{2+} triggers the release of insulin granules. Research on these pathways has relied heavily on bioimaging[23, 28]. However, integrative studies on the signal transduction networks of islets are rare, possibly due to the lack of orthogonal probes for the key components such as Ca^{2+}, mitochondria, and secreted granules.

Using our newly-developed far-red Zn^{2+} probe, it is now possible to record time-lapse, four-color and 3D fluorescence imaging of mitochondrial signal, Ca^{2+} influx, and insulin secretion in living mouse islets. We prepared transgenic mice expressing **GCaMP6f** (Ex = 488 nm), a genetically-encoded, green-emitting calcium indicator[29], under the Ins1 promoter in β-cells. Islets isolated from these mice were treated with **PK Mito Red**[30] (yellow, Ex = 561 nm) to image mitochondria with minimal phototoxicity. **PKZnFR-3** (red, Ex = 647 nm) to record insulin release from β-cells; and **Hoechst** (blue, Ex = 405 nm) to counter-stain nuclei.

The mitochondrial signal recorded with cationic **PK Mito Red** partly correlates to mitochondrial membrane potential (Figure S19). The islets were then recorded under a spinning disk confocal microscope. Four-color imaging showed that, when islets were stimulated with a high concentration of glucose for ~1 minute, the Ca^{2+} signal abruptly increased, followed by the emergence of insulin secretion puncta, meanwhile, the mitochondrial signal did not change significantly (Figure 8a, S20 and Movie 4). Furthermore, it revealed an orchestrated yet complicated relationship between Ca^{2+}, Zn^{2+} and mitochondrial signal. The whole-islet recording revealed that β-cells were highly heterogeneous in terms of mitochondrial signal, Ca^{2+} influx, and levels of insulin secretion. And this heterogeneity was seen across the entire islet at different depths (Figure 8b and Movie 5). Thanks to the minimal phototoxicity of both **PKZnFR-3** and **PK Mito Red**, the four-color recording lasted for 300 frames (15 min at 0.33 fps) without perceptible damage.

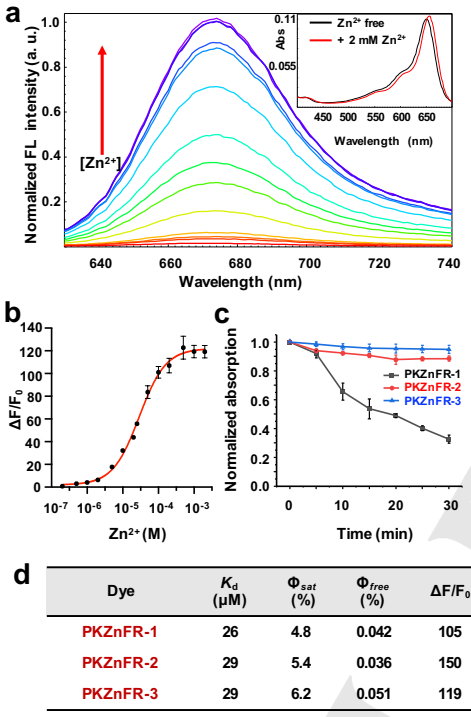

d

Dye	K_d (μM)	Φ_{sat} (%)	Φ_{free} (%)	$\Delta F/F_0$
PKZnFR-1	26	4.8	0.042	105
PKZnFR-2	29	5.4	0.036	150
PKZnFR-3	29	6.2	0.051	119

Figure 7. Characterizations of PKZnFR 1-3 *in vitro*. (a). Emission spectra of **PKZnFR-3** (1 μM) in the presence of various concentrations of free Zn^{2+} (0 to 2 mM). (*Inset*) Absorption spectra of **PKZnFR-3** (1 μM) in the presence of 0 and 2 mM free Zn^{2+}. (b). Zn^{2+} titration of **PKZnFR-3** (1 μM) as measured from its emission at 675 nm. (c). Absorbance changes of **PKZnFR-1** (black squares), **PKZnFR-2** (red circles) and **PKZnFR-3** (blue triangles) in HEPES buffer, showing the outstanding chemical stability of **PKZnFR-3**. (d). Photophysical properties of **PKZnFR 1-3**. All measurements were performed in buffers containing 100 mM HEPES (pH 7.4, $I(NaNO_3)$ = 0.1) and 0.1% DMSO as a cosolvent at 25 °C. Zero Zn^{2+} measurements were made in the presence of 10 μM TPEN. The excitation wavelength was 620 nm. Error bars denote SD; n=3.

The data generated in 4D recording prompted us to turn to computer-aided data analysis (see supporting information) to characterize the Ca^{2+} influx, mitochondrial signal, and fusion events in the whole islet (Figure 8f) and in each β-cell (Figure 8c-e). We found that the β-cells with the highest mitochondrial signal released fewer insulin granules (Figure 8c), while those with the most fusion events had relatively low mitochondrial signal (Figure 8g). Unexpectedly, those β-cells with the maximum Ca^{2+} influx had little-to-no detectable fusion events (Figure 8e); meanwhile, the Ca^{2+} influx signal of the cells with the most fusion events was not significantly higher than that of other cells (Figure 8d). These results were verified by imaging experiments on seven individual islets (Figure 8g, the complete three views in Figure S21). Of note, the physiological significance of the heterogeneous mitochondrial signal, as well as the interplay between mitochondrial signal, Ca^{2+} influx and insulin secretion in islets, represent appealing topics that are under investigation in our labs. The multi-color time-lapse imaging approach, made possible by orthogonal low-phototoxic probes, highlights the potential impact of red-shifted Zn^{2+} probes on the field of islet biology.

CONCLUSIONS

The phototoxicity of fluorescent probes, traditionally overshadowed by the photobleaching process, has been increasingly recognized as an independent bottleneck in 4D and super-resolution imaging[31]. A strategy for alleviating photodynamic damage to cells was recently developed using the conjugation of triplet-state quenchers[30]. This work showcased another parallel strategy for eliminating phototoxicity, which focused on improving the specificity of probes by tuning their polarity. Such morpholino modifications, while routine in medicinal chemistry, represent an original advance in the photo-chemical biology of rhodamine. They also resonate with the development of modern auxochromes for superior optical properties. We speculate that the next generation of probes will combine the features of twisted intramolecular charge transfer (TICT) dyes to compensate the compromised quantum yield of morpholino rhodamines[32]. This technological trend, in our opinion, exemplifies the integration of photochemistry with medicinal chemistry to enable cutting-edge bioimaging applications.

From a chemistry perspective, this work provides a new, practical synthetic route of far-red Zn^{2+} probes, the favorite window to complement genetically-encodable indicators. We plan to elaborate the transient protection/late-stage alkylation tactic to generate various probes in the far-red or even NIR window. It is noteworthy that, adding an orthogonal channel offers exponentially-expanded information in space and time, drastically enriching the analysis of an intertwining signaling network. Reminiscent to the neuroimaging field where time-lapse video data has been routinely processed using computer programs to map single neuron activities[33], Zn^{2+} biology in islets is now stepping into such digital era. To a certain extent, the chemical advances in far-red probes may leverage the integration of artificial intelligence and bioimaging, in which multiplexed biocompatible probes play an instrumental role.

The **PK Zinc** family advances the imaging of β-cell secretion on the islet level and is tailored to fit both mouse and human islet samples. These integrative imaging approaches represent a viable alternative to the traditional screening platform for active compounds. Moreover, 4D and multi-color imaging provides a system biology perspective on the cellular functions and communications in islets.

10.1002/ange.202109510

WILEY-VCH

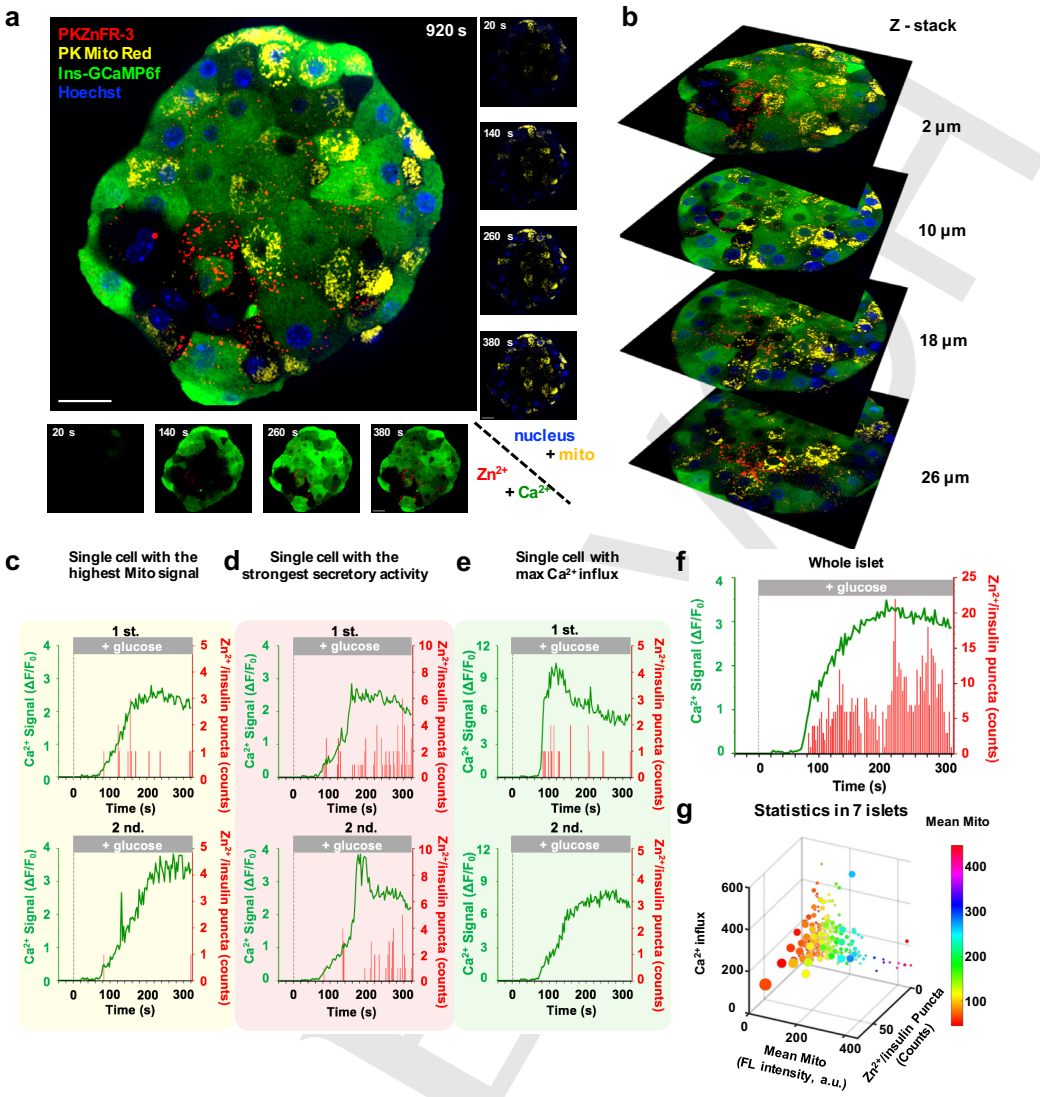

Figure 8. PKZnFR-3 enables time-lapse, four-color fluorescence imaging of mouse islets and establishes the relationships between total Ca^{2+} influx, mitochondrial signal and Zn^{2+}/insulin secretion. (a). Four-color confocal image of a mouse islet expressing **Ins-GCaMP6f** (green, Ex. = 488 nm) stained with 80 µM **Hoechst** (blue, Ex. = 405 nm), 200 nM **PK Mito Red** (yellow, Ex. = 561 nm) and 10 µM **PKZnFR-3** (Red, Ex.= 647 nm). (Main figure) snapshot at 920 s. Scale bar = 20 µm. (Right panels) Time-dependent images of the nucleus (blue, **Hoechst**) and mitochondria (yellow, **PK Mito Red**). (Lower panels) Two-color time-lapse images of green and red channels measuring dynamic changes of the Ca^{2+} and Zn^{2+}/insulin signals. (b). Z-stack of the islet with four-color images at depths of 2-26 µm. (c-f). The dynamics of Ca^{2+} signals (green curve) and fusion events (red histogram) across a whole islet (f) and representative cells with the highest mitochondrial signal (c), the strongest secretory activity (d) and the maximum Ca^{2+} influx (calculated by the area under the curve) (e) after glucose stimulation (18.2 mM). (g). Relationship of cellular Ca^{2+} influx, mitochondrial signal and fusion events in single β-cells from 7 islets. Dot size represents the number of fusion events. The color bar shows the mean fluorescence intensity of mitochondria in each cell.

Acknowledgements

This work was supported by Beijing Municipal Science & Technology Commission (Project: Z201100005320017 to Z.C.), Beijing Youth Top-notch Talent Group (Project: 7350500012 to Z.C. and L.C.), the National Natural Science Foundation of China (Project 31971375 to Z. C.; 31821091 to Z. C. and L. C.; and 81925022, 31570839, and 31327901 to L. C.; 12090053, 32088101 to C.T., 82070805 to S. W.), Peking-Tsinghua Center for Life Sciences (to Z.C. and C.T.), start-up fund from Peking University (to Z. C.), the China National Funds for Distinguished Young Scientists (8200905401 to L. C.), the National Science and Technology Major Project Program Project (2016YFA0500400 to L. C.), the Beijing Natural Science Foundation (L172003 to L. C.), National Key Research and Development Program (2020YFA0803704 to S. W.), Postdoc fellowship of Peking-Tsinghua Center for Life Sciences to X. P. and Boya postdoctoral fellowship of Peking University to H. R.. We thank Profs. Chu Wang, Zhen Yang and Jia-Hua Chen for sharing their chemistry labs, Profs. Heping Cheng and Xianhua Wang for sharing their spectrometers, Prof. Iain Bruce, Dr. Qinsi Zheng and Qi Tang for helpful discussions. We thank the High-Performance Computing Platform of Peking University and the Metabolic Mass Spectrometry Platform of IMM, Peking University. We also thank the NMR facility of National Center for Protein Sciences at Peking University for assistance with data acquisition.

Conflicts of interest

Z.C., J.Z., X.P., and Y.W. have submitted a patent application based on **PK Zinc dyes** described in this work.

Keywords: zinc• insulin secretion • fluorescent probe • biocompatibility • 4D islet physiology

[1] J. M. Berg, Y. G. Shi, *Science* **1996**, *271*, 1081-1085.
[2] A. Q. Truong-Tran, J. Carter, R. E. Ruffin, P. D. Zalewski, *Biometals* **2001**, *14*, 315-330.
[3] a) K. H. Falchuk, *Mol Cell Biochem* **1998**, *188*, 41-48; b) G. K. Andrews, *Biometals* **2001**, *14*, 223-237.
[4] B. L. Vallee, K. H. Falchuk, *Physiol. Rev.* **1993**, *73*, 79-118.
[5] C. J. Frederickson, J. Y. Koh, A. I. Bush, *Nat. Rev. Neurosci.* **2005**, *6*, 449-462.
[6] L. Silvestroni, A. Menditto, A. Modesti, S. Scarpa, *Arch. Androl.* **1989**, *23*, 97-103.
[7] C. G. Taylor, *Biometals* **2005**, *18*, 305-312.
[8] a) K. P. Carter, A. M. Young, A. E. Palmer, *Chem. Rev.* **2014**, *114*, 4564-4601; b) L. Fang, M. Watkinson, *Chemical Science* **2020**, *11*, 11366-11379; c) Y. Chen, Y. Bai, Z. Han, W. He, Z. Guo, *Chem. Soc. Rev.* **2015**, *44*, 4517-4546.
[9] a) S. C. Burdette, G. K. Walkup, B. Spingler, R. Y. Tsien, S. J. Lippard, *J. Am. Chem. Soc.* **2001**, *123*, 7831-7841; b) E. L. Que, R. Bleher, F. E. Duncan, B. Y. Kong, S. C. Gleber, S. Vogt, S. Chen, S. A. Garwin, A. R. Bayer, V. P. Dravid, T. K. Woodruff, T. V. O'Halloran, *Nat. Chem.* **2015**, *7*, 130-139; c) F. Qian, C. L. Zhang, Y. M. Zhang, W. J. He, X. Gao, P. Hu, Z. J. Guo, *J. Am. Chem. Soc.* **2009**, *131*, 1460-1468; d) K. R. Gee, Z. L. Zhou, D. Ton-That, S. L. Sensi, J. H. Weiss, *Cell Calcium* **2002**, *31*, 245-251; e) E. H. Ghazvini Zadeh, Z. Huang, J. Xia, D. Li, H. W. Davidson, W. H. Li, *Cell. Rep.* **2020**, *32*, 107904; f) S. L. Sensi, D. Ton-That, J. H. Weiss, A. Rothe, K. R. Gee, *Cell Calcium* **2003**, *34*, 281-284; g) Y. Koide, Y. Urano, K. Hanaoka, T. Terai, T. Nagano, *ACS Chem. Biol.* **2011**, *6*, 600-608.
[10] C. E. Outten, T. V. O'Halloran, *Science* **2001**, *292*, 2488-2492.
[11] B. Formby, F. Schmid-Formby, G. M. Grodsky, *Diabetes* **1984**, *33*, 229-234.
[12] Y. V. Li, *Endocrine* **2014**, *45*, 178-189.
[13] a) Z. Guo, G. H. Kim, I. Shin, J. Yoon, *Biomaterials* **2012**, *33*, 7818-7827; b) Z. Guo, G. H. Kim, J. Yoon, I. Shin, *Nat. Protoc.* **2014**, *9*, 1245-1254; c) K. Kiyose, H. Kojima, Y. Urano, T. Nagano, *J. Am. Chem. Soc.* **2006**, *128*, 6548-6549.
[14] J. Icha, M. Weber, J. C. Waters, C. Norden, *Bioessays* **2017**, *39*.
[15] D. J. Michael, R. A. Ritzel, L. Haataja, R. H. Chow, *Diabetes* **2006**, *55*, 600-607.
[16] M. Lee, B. Maji, D. Manna, S. Kahraman, R. M. Elgamal, J. Small, P. Kokkonda, A. Vetere, J. M. Goldberg, S. J. Lippard, R. N. Kulkarni, B. K. Wagner, A. Choudhary, *J. Am. Chem. Soc.* **2020**, *142*, 6477-6482.
[17] D. Li, S. Chen, E. A. Bellomo, A. I. Tarasov, C. Kaut, G. A. Rutter, W. H. Li, *Proc. Natl. Acad. Sci. USA* **2011**, *108*, 21063-21068.
[18] K. R. Gee, Z. L. Zhou, W. J. Qian, R. Kennedy, *J. Am. Chem. Soc.* **2002**, *124*, 776-778.
[19] D. Kand, P. Liu, M. X. Navarro, L. J. Fischer, L. Rousso-Noori, D. Friedmann-Morvinski, A. H. Winter, E. W. Miller, R. Weinstain, *J. Am. Chem. Soc.* **2020**, *142*, 4970-4974.
[20] E. R. H. Walter, M. A. Fox, D. Parker, J. A. G. Williams, *Dalton Trans.* **2018**, *47*, 1879-1887.
[21] S. Iyoshi, M. Taki, Y. Yamamoto, *Org Lett* **2011**, *13*, 4558-4561.
[22] J. Cantley, F. M. Ashcroft, *BMC Biol.* **2015**, *13*, 33.
[23] S. Seino, T. Shibasaki, K. Minami, *J. Clin. Invest.* **2011**, *121*, 2118-2125.
[24] J. Li, Q. Yu, P. Ahooghalandari, F. M. Gribble, F. Reimann, A. Tengholm, E. Gylfe, *FASEB J.* **2015**, *29*, 3379-3388.
[25] a) T. Egawa, K. Hanaoka, Y. Koide, S. Ujita, N. Takahashi, Y. Ikegaya, N. Matsuki, T. Terai, T. Ueno, T. Komatsu, T. Nagano, *J. Am. Chem. Soc.* **2011**, *133*, 14157-14159; b) C. Deo, S. H. Sheu, J. Seo, D. E. Clapham, L. D. Lavis, *J. Am. Chem. Soc.* **2019**, *141*, 13734-13738; c) O. Murata, Y. Shindo, Y. Ikeda, N. Iwasawa, D. Citterio, K. Oka, Y. Hiruta, *Anal. Chem.* **2020**, *92*, 966-974; d) G. Lukinavicius, L. Reymond, K. Umezawa, O. Sallin, E. D'Este, F. Gottfert, H. Ta, S. W. Hell, Y. Urano, K. Johnsson, *J. Am. Chem. Soc.* **2016**, *138*, 9365-9368.
[26] a) S. L. Gibson, J. J. Holt, M. Ye, D. J. Donnelly, T. Y. Ohulchanskyy, Y. You, M. R. Detty, *Bioorg. Med. Chem.* **2005**, *13*, 6394-6403; b) J. Zhang, N. R. Myllenbeck, T. L. Andrew, *Org. Lett.* **2017**, *19*, 210-213.
[27] T. Myochin, K. Hanaoka, S. Iwaki, T. Ueno, T. Komatsu, T. Terai, T. Nagano, Y. Urano, *J. Am. Chem. Soc.* **2015**, *137*, 4759-4765.
[28] N. R. Johnston, R. K. Mitchell, E. Haythorne, M. P. Pessoa, F. Semplici, J. Ferrer, L. Piemonti, P. Marchetti, M. Bugliani, D. Bosco, E. Berishvili, P. Duncanson, M. Watkinson, J. Broichhagen, D. Trauner, G. A. Rutter, D. J. Hodson, *Cell Metab.* **2016**, *24*, 389-401.
[29] T. W. Chen, T. J. Wardill, Y. Sun, S. R. Pulver, S. L. Renninger, A. Baohan, E. R. Schreiter, R. A. Kerr, M. B. Orger, V. Jayaraman, L. L. Looger, K. Svoboda, D. S. Kim, *Nature* **2013**, *499*, 295-300.
[30] Z. Yang, L. Li, J. Ling, T. Liu, X. Huang, Y. Ying, Y. Zhao, Y. Zhao, K. Lei, L. Chen, Z. Chen, *Chem. Sci.* **2020**, *11*, 8506-8516.
[31] a) P. Montero Llopis, R. A. Senft, T. J. Ross-Elliott, R. Stephansky, D. P. Keeley, P. Koshar, G. Marques, Y. S. Gao, B. R. Carlson, T. Pengo, M. A. Sanders, L. A. Cameron, M. S. Itano, *Nat. Methods* **2021**, ASAP, doi: 10.1038/s41592-021-01156-w; b) S. C. Boggess, S. S. Gandhi, B. R. Benlian, E. W. Miller, *J. Am. Chem. Soc.* **2021**, *143*, 11903-11907.
[32] a) J. B. Grimm, B. P. English, J. Chen, J. P. Slaughter, Z. Zhang, A. Revyakin, R. Patel, J. J. Macklin, D. Normanno, R. H. Singer, T. Lionnet, L. D. Lavis, *Nat. Methods* **2015**, *12*, 244-250; b) Z. Ye, W. Yang, C. Wang, Y. Zheng, W. Chi, X. Liu, Z. Huang, X. Li, Y. Xiao, *J. Am. Chem. Soc.* **2019**, *141*, 14491-14495; c) X. Liu, Q. Qiao, W. Tian, W. Liu, J. Chen, M. J. Lang, Z. Xu, *J. Am. Chem. Soc.* **2016**, *138*, 6960-6963; d) X. Lv, C. Gao, T. Han, H. Shi, W. Guo, *Chem. Commun. (Camb)* **2020**, *56*, 715-718.
[33] a) A. S. Abdelfattah, T. Kawashima, A. Singh, O. Novak, H. Liu, Y. Shuai, Y. C. Huang, L. Campagnola, S. C. Seeman, J. Yu, J. Zheng, J. B. Grimm, R. Patel, J. Friedrich, B. D. Mensh, L. Paninski, J. J. Macklin, G. J. Murphy, K. Podgorski, B. J. Lin, T. W. Chen, G. C. Turner, Z. Liu, M. Koyama, K. Svoboda, M. B. Ahrens, L. D. Lavis, E. R. Schreiter, *Science* **2019**, *365*, 699-704; b) M. A. Gonzalez, A. S. Walker, K. J. Cao, J. R. Lazzari-Dean, N. S. Settineri, E. J. Kong, R. H. Kramer, E. W. Miller, *J. Am. Chem. Soc.* **2021**, *143*, 2304-2314.

10.1002/ange.202109510

WILEY-VCH

RESEARCH ARTICLE

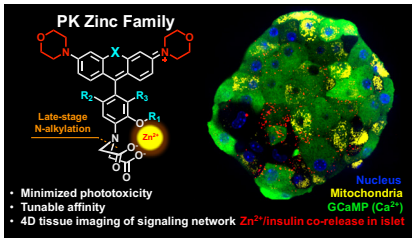

We synthesized a new class of red- and far-red-emitting Zn^{2+} probes with minimal phototoxicity, μM affinities and high turn-on ratios. Tailored for 4D, long-term and multiple-color recording of Zn^{2+}/insulin co-secretion in β-cells and islets, the new probes promise to unveil the spatial-temporal regulation of islet endocrinology.